DsrMKJOP is the terminal reductase complex in anaerobic sulfate respiration

Ana C. C. Barbosa[‡], Sofia S. Venceslau[‡]*, Inês A. C. Pereira*

Instituto de Tecnologia Química e Biológica António Xavier, Universidade Nova de Lisboa, 2780-156 Oeiras, Portugal

[‡]These authors contributed equally to this work

*Corresponding authors: ipereira@itqb.unl.pt
sofiavenceslau@gmail.com

A.C.C.B.: ORCID ID: 0000-0003-3577-2927
S.S.V.: ORCID ID: 0000-0001-8774-1351
I.A.C.P.: ORCID ID: 0000-0003-3283-4520

KEYWORDS

Sulfur metabolism; Dissimilatory sulfite reductase; Sulfate reducing bacteria; DsrAB, DsrC

The authors have no competing interests.

ABSTRACT

Microbial dissimilatory sulfate reduction is a key process in the Earth biogeochemical sulfur cycle. In spite of its importance to the sulfur and carbon cycles, industrial processes and human health, it is still not clear how reduction of sulfate to sulfide is coupled to energy conservation. A central step in the pathway is the reduction of sulfite by the DsrAB dissimilatory sulfite reductase, which leads to the production of a DsrC-trisulfide. A membrane-bound complex, DsrMKJOP, is present in most organisms that have DsrAB and DsrC, and its involvement in energy conservation has been inferred from sequence analysis, but its precise function was so far not determined. Here, we present studies revealing that the DsrMKJOP complex of the sulfate reducer *Archaeoglobus fulgidus* works as a menadiol:DsrC-trisulfide oxidoreductase. Our results reveal a close interaction between the DsrC-trisulfide and the DsrMKJOP complex and show that electrons from the quinone pool reduce consecutively the DsrM hemes *b*, the DsrK noncubane $[4Fe\text{-}4S]^{3+/2+}$ catalytic center, and finally the DsrC-trisulfide with concomitant release of sulfide. These results clarify the role of this widespread respiratory membrane complex and indicate that DsrMKJOP will provide the missing link to energy conservation by generating a *proton motive force* across the membrane in the last step of dissimilatory sulfate reduction.

Significance Statement

Dissimilatory sulfate reduction (DSR) is a vital microbial process in anoxic environments, namely in sulfate-rich marine sediments that harbor a vast microbial ecosystem. DSR drives the global biogeochemical sulfur cycle and is crucial in remineralization of organic matter on the seafloor. It also has huge environmental impact by preventing release of the greenhouse gas methane from these sediments, through its oxidation coupled to sulfate reduction. Despite its high ecological importance, it is still not clear how microorganisms derive energy to grow through DSR. Here, we disclose the physiological function of a widespread membrane complex in DSR, showing it acts as the terminal reductase in the respiratory chain and providing important insights into how sulfate/sulfite reduction is linked to energy conservation.

53 **INTRODUCTION**

54 Sulfur is a key element for life, mainly due to its chemical versatility and ability to switch between several
55 biologically relevant oxidation states, ranging from -2, as in hydrogen sulfide (H_2S), up to +6, as in sulfate
56 (SO_4^{2-}). A critically important microbial process in the biogeochemical sulfur cycle is dissimilatory sulfate
57 reduction (DSR) driven by anaerobic bacteria and archaea, in which the reduction of sulfate to hydrogen
58 sulfide is linked to energy conservation (1, 2). This process has particular impact in marine sediments,
59 accounting for up to 50% of carbon mineralization in the sea floor (3), and preventing methane emissions
60 through its contribution to anaerobic methane oxidation (4, 5). Despite being a very ancient bioenergetic
61 pathway (6), it is still not clear how sulfate reducers are able to conserve energy during sulfate respiration.
62 In DSR, a central step is the reduction of sulfite, performed by the dissimilatory sulfite reductase DsrAB
63 and its physiological partner DsrC, which mediate a four-electron reduction of sulfite to zero-valent sulfur
64 in the form of a trisulfide formed between two conserved cysteines of DsrC (7–9). The reduction of the
65 DsrC-trisulfide to hydrogen sulfide is thought to derive electrons from the quinone pool via the
66 membrane-bound DsrMKJOP complex, pointing to a critical role of this complex in energy conservation
67 (7, 10, 11). The Dsr proteins, namely DsrAB, DsrC and DsrMKJOP, are widespread in the microbial world,
68 being also present in phototrophic and chemotrophic sulfur-oxidizing organisms where they are involved
69 in sulfite oxidation (12, 13), and in many organisms capable of sulfur, thiosulfate, sulfite or
70 organosulfonates reduction, and in sulfur disproportionators (14, 15). However, there is still no concrete
71 evidence demonstrating the physiological function of the DsrMKJOP complex.

72 The DsrMKJOP complex was first isolated and characterized from *Archaeoglobus fulgidus* (16), then from
73 *Desulfovibrio desulfuricans* (11), and later from *Allochromatium vinosum* (17), where this complex has
74 been shown to be essential for sulfur globule oxidation (18). This transmembrane complex contains two
75 periplasmic subunits (DsrJ and DsrO), two integral membrane subunits (DsrM and DsrP) and a cytoplasmic
76 subunit (DsrK), and appears to be composed of a combination of two modules, DsrMK and DsrJOP (19).
77 The MK module is homologous to the membrane-bound HdrED heterodisulfide reductase (Hdr) from
78 methanogens (20–22), comprising a quinone-interacting membrane diheme cytochrome *b* DsrM, with
79 both hemes displaying His/His coordination, and an iron-sulfur subunit DsrK predicted to have two
80 canonical $[4Fe\text{-}4S]^{2+/1+}$ clusters, and one noncubane $[4Fe\text{-}4S]^{3+/2+}$ cluster (11). The noncubane cluster is
81 predicted on the basis of a conserved five-cysteine motif $CX_nCCGX_nCX_2C$ (the CCG motif) (23), which was
82 identified to bind the catalytic noncubane cluster for heterodisulfide reduction in the homologous HdrD
83 (16). The DsrJOP module contains DsrP, an integral membrane subunit with ten predicted transmembrane
84 helices, and DsrO, an iron-sulfur subunit predicted to coordinate three to four $[4Fe\text{-}4S]^{2+/1+}$ clusters, which
85 together resemble the quinone-interacting NrfCD module widespread in bacterial oxidoreductases (24).
86 DsrJ is a membrane-anchored triheme cytochrome *c*, where each heme is proposed to have distinct axial
87 coordination: His/His, His/Met and His/Cys (11, 25). The His/Cys heme *c* coordination is very unusual but
88 is also found in SoxXA (26), TdsA (27) and PufC (28), which are involved in thiosulfate oxidation and/or
89 electron transfer, suggesting that DsrJ could have a catalytic role in sulfur redox chemistry. Notably, the
90 DsrJOP module is absent in many Gram-positive (Firmicutes) and archaeal sulfate reducers (19), and so
91 does not seem to be essential. In contrast, the DsrMK proteins are present in all organisms containing
92 DsrAB and DsrC, often encoded in the same operon and sometimes with multiple copies in the genome,
93 which suggests this is the minimum functional module of this respiratory complex (19). Based on its

94 similarity to HdrED, the DsrMK module was proposed to catalyze the reduction of DsrC-trisulfide to
95 hydrogen sulfide through the oxidation of the quinone pool (7, 10, 11, 29). However, the presence of the
96 DsrJOP module suggests that there may be a more elaborate mechanism (7). Both DsrM and DsrP are
97 homologous to quinone-interacting proteins, and the presence of two putative quinone-binding sites led
98 to the suggestion that a quinone cycle between the DsrMK and DsrJOP modules may be present (10).

99 The X-ray structure of the soluble HdrABC-MvhAGD complex from the methanogenic archaeon
100 *Methanothermococcus thermolithotrophicus*, comprising the MvhAGD hydrogenase and the HdrABC
101 heterodisulfide reductase, provided the first structural insights into the two noncubane $[4Fe\text{-}4S]^{3+/2+}$
102 clusters present in the active site of HdrB, and how they mediate the reduction of CoM-S-S-CoB
103 heterodisulfide (30). Each noncubane cluster is ligated by five cysteines from the predicted CCG motif.
104 There are two such motifs in both HdrB and HdrD, the catalytic subunits of the two different types of Hdrs
105 in methanogens. Cleavage of the CoM-S-S-CoB disulfide bond has been suggested to involve the two
106 noncubane clusters in a homolytic mechanism, along with binding of each substrate to one of the clusters
107 (30). Remarkably, only one CCG motif is present in DsrK, raising the question of how this protein may
108 operate with a single noncubane cluster. Recently, studies of the noncubane $[4Fe\text{-}4S]^{3+/2+}$ cluster in the
109 HdrB protein from *Desulfovibrio vulgaris* Hildenborough revealed that this cluster can adopt "closed" and
110 "open" conformations corresponding to the substrate-free and substrate-bound forms, respectively (31),
111 suggesting that cluster flexibility may be important for binding the DsrC-trisulfide in the active site of its
112 homolog, DsrK.

113 Overall, unraveling the role of the DsrMKJOP complex and its link to DsrC-trisulfide reduction and
114 corresponding energy conservation mechanism is a major challenge in understanding dissimilatory sulfur
115 metabolism. In the present study, we provide evidence for the activity of the DsrMKJOP complex as a
116 menadiol:DsrC-trisulfide oxidoreductase, clarifying the functional role of this membrane complex in the
117 final step of the sulfate respiratory chain, where it is likely coupled to energy conservation.
118

119 **RESULTS AND DISCUSSION**

120 **DsrMKJOP isolation and reduction with Menadiol**

121 The DsrMKJOP transmembrane complex was purified with DDM as solubilizing detergent from
122 membranes of the thermophilic archaeon *A. fulgidus,* by adapting the protocol previously reported by
123 Mander *et al.* (16). The DsrMKJOP complex is the only heme-containing membrane complex in *A. fulgidus*
124 (19), which facilitates its purification compared with other sulfate reducers, such as *D. desulfuricans* (11).
125 In *A. fulgidus*, the predicted molecular mass for each subunit of the complex is 38.4 kDa (DsrM, locus tag:
126 AF0501), 64.4 kDa (DsrK, AF0502), 16.7 kDa (DsrJ, AF0503), 30.5 kDa (DsrO, AF0499), and 44.2 kDa (DsrP,
127 AF0500). The purified complex displayed four bands on a Tricine-SDS-PAGE gel (**Figure S1**) with apparent
128 molecular masses of 61, 31, 28, and 17 kDa, in line with the report by Mander *et al.* (16). The 17 kDa band
129 was identified as a cytochrome *c* (DsrJ) by heme-staining, and the other bands were assigned as DsrK (61
130 kDa), DsrM (31 kDa), DsrO (28 kDa), based on previous identifications (11, 16). As reported before, DsrP
131 is not detected by SDS-PAGE (11, 16) because it is a highly hydrophobic subunit (ten predicted
132 transmembrane helices), which hinders its migration in the gel.

133 The UV-visible spectrum of the as-purified DsrMKJOP (oxidized state) is dominated by absorption maxima
134 at 280, 410 and 527 nm (**Figure 1A**), confirming the presence of hemes. Upon reduction, the Soret peak
135 shifts to 420 nm, and the β- and α-bands are observed at 524 and 557 nm, respectively, which is in line
136 with previously reported spectra of DsrMKJOP from *A. fulgidus* (16) and *D. desulfuricans* (11). The α-band
137 is quite broad supporting the presence of hemes *b* and *c*. Addition of menadiol reduced 38% of the total
138 hemes as compared with full reduction by dithionite. This corresponds to approximately two hemes
139 reduced, and since hemes *b* typically have higher redox potentials than hemes *c,* this likely corresponds
140 to the two predicted hemes *b* in the quinone-interacting DsrM membrane subunit. A similar result was
141 reported by Pires *et al.* (11), where 40% of hemes belonging to the *D. desulfuricans* DsrMKJOP were also
142 reduced upon incubation with menadiol.

143 The electron paramagnetic resonance (EPR) spectrum of the as-purified *A. fulgidus* DsrMKJOP shows an
144 intense rhombic signal characteristic of a noncubane $[4Fe\text{-}4S]^{3+/2+}$ cluster in the oxidized state, with *g*-
145 values of 2.025, 1.995 and 1.947 (**Figure 1B**). This EPR signature was first observed in heterodisulfide
146 reductases from methanogens (upon addition of HS-CoM or HS-CoB), with *g*-values of 2.013, 1.991 and
147 1.938 for HdrABC from *Methanothermobacter marburgensis* and 2.012, 1.993 and 1.946 for HdrED from
148 *Methanosarcina barkeri* (41, 42), both of which possess two noncubane $[4Fe\text{-}4S]^{3+/2+}$ catalytic centers
149 involved in mediating heterodisulfide (CoM-S-S-CoB) reduction in two one-electron steps (22, 43). The
150 previously reported *g*-values of *A. fulgidus* DsrMKJOP were 2.031, 1.994 and 1.941 (16), while in *D.*
151 *desulfuricans* DsrMKJOP the *g*-values were 2.027, 1.991 and 1.943 (11). Given the similarity of DsrK to
152 HdrD, the noncubane $[4Fe\text{-}4S]^{3+/2+}$ cluster present in DsrK is likely involved in thiol/disulfide chemistry,
153 suggesting that DsrK is the catalytic subunit of the DsrMKJOP complex. Upon incubation with menadiol
154 under anaerobic conditions, the intensity of the rhombic signal decreased by 85%, revealing a pathway
155 for electron transfer from the hemes *b* of DsrM to the noncubane $[4Fe\text{-}4S]^{3+/2+}$ cluster of DsrK. The redox
156 potential of the noncubane center in *A. fulgidus* DsrK was previously determined to be +90 mV (16), which
157 agrees with its reduction by menadiol (midpoint potential of approx. -70 mV).

158

159 **The DsrC-trisulfide interacts strongly with DsrMKJOP**

160 In *A. vinosum*, coelution upon protein purification suggested that DsrK interacts with DsrC (17). Following
161 our identification of the DsrC-trisulfide as the product of sulfite reduction by DsrAB, we proposed that this
162 is the actual substrate for the DsrMKJOP complex (7). To assess if there is a protein-protein interaction
163 between the DsrC-trisulfide and the DsrMKJOP complex, surface plasmon resonance (SPR) was initially
164 used. SPR is a highly sensitive technique for studying protein-protein interactions, without the need for
165 labeling. The *A. fulgidus* DsrC-trisulfide was produced by *in vitro* enzymatic reaction using DsrAB from the
166 same organism, as described in Santos *et al.* (7). The DsrC-trisulfide thus produced was immobilized on a
167 nitrilotriacetic acid (NTA) sensor chip by the N-terminal His-tag, and the interaction was studied with
168 increasing concentrations of DsrMKJOP complex (**Figure 2**). A strong interaction was observed between
169 the two proteins, which could be detected even at low concentrations of the membrane complex. Steady-
170 state conditions could not be achieved (even by increasing the association time), which means that no
171 kinetic model could fit the experimental data, and so the association and dissociation rate constants could
172 not be obtained. Nevertheless, an estimate for the equilibrium dissociation constant (K_D) of 200 ± 27 nM
173 was derived from duplicate sensorgrams using the maximum response reached. This K_D confirms a strong

interaction between the DsrC-trisulfide and the DsrMKJOP complex (strong interactions are in the nanomolar range, or even lower as in the case of high-affinity antibodies), supporting the DsrC-trisulfide as a possible substrate for the membrane-bound DsrMKJOP complex. The SPR data were obtained at 25 °C, whereas a higher temperature (as used in the activity assays) should favor the association and dissociation rates of DsrC-trisulfide to DsrMKJOP complex since *A. fulgidus* is a thermophile, suggesting that the actual K_D at physiological temperatures may be somewhat different, and possibly even lower.

The DsrC-trisulfide is reduced by DsrMKJOP

Given that menadiol can reduce the noncubane $[4Fe\text{-}4S]^{3+/2+}$ catalytic center of DsrK, and that the DsrC-trisulfide interacts with DsrMKJOP complex, we tested whether the DsrC-trisulfide can serve as substrate and electron acceptor for the menadiol-reduced DsrMKJOP complex. Menadiol:DsrC-trisulfide oxidoreductase activity by the DsrMKJOP complex was thus measured. These experiments confirmed a fast oxidation of menadiol (measured by menadione formation at 270 nm) in the presence of the DsrC-trisulfide with a specific activity of 85.5 ± 5.4 mU/mg, assuming DsrMKJOP as a 5-subunit monomer (200 kDa) (**Figure 3A**). In control reactions without DsrMKJOP, menadiol or DsrC-trisulfide no activity was detected. In addition, sequential additions of DsrC-trisulfide, after the reaction has stopped, trigger a new phase of menadiol oxidation confirming it had stopped due to substrate depletion (**Figure 3B**).

The redox state of DsrC, before and after the reaction, was analyzed by a gel-shift assay using MalPEG, which selectively labels cysteine thiol groups (7, 37). In this assay, the DsrC-trisulfide presents no shift in the gel as it cannot bind MalPEG, whereas the reduced form binds one or two MalPEG molecules, as the last Cys_A is more accessible for labeling than Cys_B (Cys^{114} and Cys^{103} in *A. fulgidus*, respectively) (7, 37). At time zero (T_0), most DsrC shows no shift, as expected for the trisulfide, but a small amount of reduced species is present, as revealed by labeling for one MalPEG, due to incomplete production of DsrC-trisulfide by DsrAB (**Figure 3C**). After the enzymatic reaction (T_f), most DsrC is now in the reduced form, as revealed by the shift for one (Cys_A) and two labeled cysteines (Cys_A and Cys_B) (**Figure 3C**). In the control experiments, without DsrMKJOP or menadiol, DsrC remains in the oxidized DsrC-trisulfide state. Using the MalPEG assay to follow the reaction in time, the decrease in the DsrC-trisulfide band and increase in the band for reduced, doubly labeled DsrC, is clearly seen (**Figure 3D**). Increasing concentrations of menadiol for the same reaction time also increase the extent of reaction (**Figure 3E**). As a control, reduced DsrC was tested as a substrate for DsrMKJOP under the same conditions. In this case, no activity is observed (**Figure S2A**), as expected, and the MalPEG assay confirms the reduced state of DsrC in the beginning and end of the experiment (**Figure S2B).**

Finally, the redox state of DsrC cysteines was also characterized by peptide mass fingerprinting after protein digestion with Asp-N endoproteinase, which gives rise to a small peptide containing both Cys_A and Cys_B, followed by alkylation with iodoacetamide (IA), which adds 57 Da per reduced cysteine (7). In reduced DsrC, the C-terminal peptide ^{101}DA**C**RIAGLPKPTG**C**V^{115} has a mass of 1498.7 Da (7), and upon alkylation, a peptide with 1614.9 Da is detected (**Figure 4A**). In the DsrC-trisulfide formed by reaction with DsrAB, the C-terminal peptide shows a mass increase of 32 Da, 1530.7 Da, which remains unaltered by alkylation with IA (**Figure 4B**). A small amount of unreacted IA-labelled DsrC is still detected in this sample (1614.8 Da), as well as a species that does not react with IA (1498.8) and likely corresponds to DsrC with a disulfide bond between the two Cys. It should be noted that the peak intensities are not directly

215 correlated with relative amounts, as they depend on the different ionization properties of each peptide.
216 As expected, analysis of the DsrC peptide after the reaction with DsrMKJOP, reveals the disappearance of
217 the DsrC-trisulfide peak at 1530.7 Da, and the increase of the 1614.8 Da peak characteristic of reduced
218 DsrC, where two cysteines react with IA (**Figure 4C**).

219

220 **Sulfide is the product of DsrMKJOP catalysis**

221 The products of DsrC-trisulfide reduction by the DsrMKJOP complex should be sulfide and reduced DsrC
222 (**Figure 5A**). To quantify the sulfide released during DsrMKJOP catalysis, the reaction was performed with
223 increasing concentrations of DsrC-trisulfide. These kinetic studies showed an increase in the length of the
224 reaction with increasing substrate concentrations (**Figure 5B**), but not an increase in reaction rate. This
225 indicates that the concentrations used are already saturating and that the Michaelis-Menten constant
226 (K_M) for the DsrC-trisulfide is probably in the nM range, in agreement with the measured K_D. The reaction
227 rates slow down as the substrate becomes exhausted. The product sulfide, quantified by HPLC as the
228 monobromobimane fluorescent derivative, increases linearly with increasing DsrC-trisulfide
229 concentrations (**Figure 5C**), although in sub-stoichiometric amounts (40 to 50%). This can be explained by
230 two factors: the partial escape of hydrogen sulfide to the gas phase at pH 7.0, made worse by the high
231 temperature required for the DsrMKJOP assay, and also by a degree of uncertainty associated with
232 quantification of the DsrC-trisulfide. This quantification was performed indirectly using the BCA (for
233 protein quantification) and DTNB (for thiol quantification) assays, by the amount of reduced DsrC
234 remaining in samples of the DsrC-trisulfide. However, we observed by mass spectrometry (MS) that upon
235 production of the DsrC-trisulfide some part of DsrC is in the disulfide state and is not alkylated by IA (peak
236 1498.8 Da in **Figure 4B and 4C**) and thus is also not quantified by DTNB derivatization, generating an
237 uncertainty in the actual level of DsrC-trisulfide present in the samples. Nevertheless, taken globally these
238 results show clearly that DsrMKJOP can catalyze full reduction of the DsrC-trisulfide to sulfide using
239 menadiol, finally clarifying the functional role of this respiratory complex in dissimilatory sulfite reduction.

240

241 **Insights into the catalytic mechanism of DsrMKJOP**

242 A catalytic mechanism for heterodisulfide reduction by Hdrs has been proposed based on the structure of
243 HdrABC with substrate bound, where the CoM-S-S-CoB heterodisulfide binds between the two noncubane
244 $[4Fe\text{-}4S]^{3+/2+}$ clusters and is homolytically cleaved (30). The thyil radicals formed may be stabilized by
245 coordination with the reduced $[4Fe\text{-}4S]^{2+}$ clusters, leading to the binding of the CoM and CoB sulfurs to
246 the two $[4Fe\text{-}4S]^{3+}$ clusters, resulting in the "open" conformation of the clusters (31). Two consecutive
247 single-electron reduction steps release CoB-SH and CoM-SH (30, 31). However, the catalytic mechanism
248 of the DsrMKJOP complex is likely different since it coordinates a single noncubane $[4Fe\text{-}4S]^{3+/2+}$ cluster in
249 DsrK instead of the two found in HdrD and HdrB (**Figure S3**). Interestingly, in many DsrK proteins from
250 different sulfate reducers the last cysteine of the CCG motif for binding this cluster is replaced by a
251 conserved aspartate (**Figure S4**). In *A. fulgidus*, the DsrK protein of the DsrMKJOP complex (AF0502) and
252 another homolog (AF0543) have this aspartate, whereas two other DsrK homologs (AF0544 and AF0547),
253 encoded in *dsrMK* arrangements, have a cysteine, suggesting that both residues may be functional. In
254 addition, one of the conserved cysteines from the missing noncubane cluster (Cys^{329} in *A. fulgidus*
255 numbering) is strictly conserved in DsrK proteins and is likely involved in the catalytic mechanism of DsrC-

256 trisulfide reduction. This cysteine is part of a conserved GECGH sequence motif that is highly conserved in
257 DsrK from several organisms (**Figure S4**) and is one of the cysteines from the second CCG signature motif
258 in HdrD and HdrB (**Figure S3**). A similar motif (ECGLH), present in APS and PAPS reductases, includes a
259 redox-active catalytic cysteine (44). Other proteins from sulfate reducers, homologous to DsrK and HdrD,
260 such as HmcF from the HmcABCDEF complex (19, 24, 45) and TmcB from the TmcABCD complex (46) also
261 contain only one CCG motif and this conserved cysteine in a T/GECGH motif (**Figure S3**), suggesting that
262 this cysteine is probably essential for disulfide reduction catalysis. The Hmc and Tmc complexes are both
263 transmembrane complexes with a similar architecture to the DsrMKJOP complex, but they are not present
264 in *A. fulgidus* (19). Interestingly, the characteristic EPR signal of the noncubane $[4Fe\text{-}4S]^{3+}$ cluster was
265 initially reported for the methanogenic HdrB and HdrD only in the presence of HS-CoM or HS-CoB (41–
266 43), which bind to the cluster, whereas for DsrK and TmcB proteins this signal is observed in the as-isolated
267 protein, in the absence of any added substrate (11, 16, 46). This could suggest that this conserved cysteine
268 might be binding the cluster and generating the open $S = ½$ conformation. However, for the recombinant
269 HdrB protein produced in *E. coli* the signal for the noncubane cluster was visible already in the absence of
270 substrate (23).
271 In methanogens, the redox potential of the CoM-S-S-CoB heterodisulfide has been determined to be $E^{0\prime}$=-
272 143 ± 10 mV vs. SHE (47), which is more positive than that of typical disulfides such as glutathione and
273 cysteine. It is also more positive than the potential of methanophenazine ($E^{0\prime}$=-165 ± 6 mV), the
274 membrane-associated quinone-like redox carrier that is the electron donor to HdrED (47). The redox
275 potential of the DsrC-trisulfide is unknown, so it is not clear whether its reduction by menaquinol ($E^{0\prime}$ ~ -
276 70 mV) is thermodynamically favorable. Protein disulfide bonds are known to span a wide range of
277 potentials. For example, *A. fulgidus* proteins from the thioredoxin superfamily have potentials ranging
278 from -32 mV to -309 mV (pH 7.0) (48). A value of -346 mV (pH 7.0, vs. SHE) has been reported for several
279 organic water-soluble trisulfides (49), but we know of no reports for redox potentials of protein-bound
280 trisulfides, so it is very difficult to estimate the redox potential of the DsrC trisulfide. We tested the
281 chemical reduction of this species by different chemical reducing agents, and surprisingly none of them,
282 not even those with very low redox potential, could reduce the DsrC-trisulfide as analyzed with the
283 MalPEG shift assay (**Figure S5**). Moreover, MS confirmed the intact state of the DsrC-trisulfide after
284 reduction with dithionite, TCEP and DTT (**Table S1**). This unexpected result suggests that the DsrC-
285 trisulfide can only be reduced by the DsrMKJOP complex. The fact that it cannot be chemically reduced
286 could suggest that it has a low redox potential, which could increase upon interaction with the DsrMKJOP
287 complex, but it is also possible that the reduction of the trisulfide is not thermodynamically, but kinetically
288 prevented, i.e. that the reaction has a high activation energy and occurs only when it is enzymatically
289 catalyzed. This sort of argument has been put forward by Flohé and coworkers in discussing the
290 glutathione redox potential and its physiological significance (50, 51). Such kinetic impediment for
291 reduction of the DsrC-trisulfide, which may be based on steric inaccessibility of the trisulfide, makes sense
292 considering that this species is likely to face a considerable intracellular sulfide concentration.
293 Nevertheless, the full reduction of the DsrC-trisulfide, as observed by MS, and the increasing production
294 of sulfide upon reaction of DsrMKJOP and menadiol with increasing concentrations of DsrC-trisulfide
295 confirm that its reduction by this menaquinol analog does occur. This reaction could, in principle, only
296 involve the DsrMK subunits in analogy to HdrED, with DsrM as the menaquinol-oxidizing subunit that

297 transfers electrons to DsrK for trisulfide reduction, and in fact, in many organisms only these two subunits
298 are present (2, 19). This leaves the function of the DsrJOP subunits as an enigma.

299 It has been suggested that the DsrJ cytochrome could react with a periplasmic sulfur substrate (11, 16,
300 25), due to the presence of the unusual His/Cys heme coordination that is also present in SoxXA involved
301 in thiosulfate oxidation (52) or in TsdA thiosulfate dehydrogenase (27). We tested both thiosulfate and
302 sulfite as electron donors to the complex and could not detect any activity with menadione and/or DsrC-
303 trisulfide as electron acceptors, and sulfite actually decreased the rate of DsrC-trisulfide reduction by
304 DsrMKJOP (**Figure S6**). Since the DsrJOP module is not essential for some organisms, a hypothesis is that
305 its role is to increase the energetic efficiency of the DsrMKJOP complex vs. the DsrMK version. We have
306 previously suggested that the DsrMK and DsrJOP modules could be involved in some form of proton-
307 translocating quinone cycling, as present in the bc_1 complex, possibly involving quinone-based electron
308 bifurcation (10). Alternatively, the DsrJOP module may allow for proton pumping upon DsrC-trisulfide
309 reduction. Notably, the DsrOP proteins form a quinone-interacting redox module that is widespread in
310 bacterial oxidoreductases (24, 53), and some proteins of the DsrP family may be involved in proton
311 pumping, such as the alternative complex III (54, 55) and the reductive dehalogenase complex (56).
312 In conclusion, our results are a major step forward in the molecular understanding of dissimilatory sulfur
313 metabolism by identifying the function of the DsrMKJOP complex, showing that it interacts with the DsrC-
314 trisulfide and acts as a menadiol:DsrC-trisulfide oxidoreductase that produces sulfide. The architecture of
315 the DsrMKJOP complex indicates that it is quite an elaborate machine and further studies will be essential
316 to understand its molecular mechanism and how it is coupled to energy conservation.
317

318 **MATERIALS AND METHODS**

319 **Purification of *A. fulgidus* DsrMKJOP**

320 *A. fulgidus* VC-16 (DSM 4304) was grown in sulfate-thiosulfate-lactate medium in 300 L fermenter at 83
321 °C, as previously described (32), without addition of dithionite. Frozen cells were resuspended in 50 mM
322 potassium phosphate buffer (KPi) pH 7.0, 10% (v/v) glycerol, homogenized and disrupted in an APV Model
323 2000 Homogenizer at 80 MPa in the presence of DNase (Sigma-Aldrich) and cOmplete™ protease inhibitor
324 cocktail (Roche). The cell lysate was centrifuged at 7930 x *g* for 20 min at 4 °C, followed by
325 ultracentrifugation at 138000 x *g* for 2 h at 4 °C. The supernatant (soluble extract) was used to isolate *A.*
326 *fulgidus* DsrAB (see below). The pellet (membrane extract) was solubilized with gentle stirring overnight
327 at 4 °C in 50 mM potassium phosphate buffer pH 7.0, 10% (v/v) glycerol, and 2% (w/v) n-dodecyl β-D-
328 maltoside (DDM, Glycon Biochemicals GmbH). The solubilized membrane proteins were separated by
329 ultracentrifugation at 138000 x *g* for 2 h at 4 °C, and the membrane pellet was used for a second
330 solubilization for 5 h with gentle stirring at 4 °C, followed by a third ultracentrifugation step under the
331 same conditions. The pooled solubilized membrane proteins were loaded into a Q-Sepharose high
332 performance column (2.6 x 10.0 cm, Amersham Pharmacia Biotech) equilibrated with buffer A (50 mM
333 KPi pH 7.0, 10% (v/v) glycerol, 0.1% (w/v) DDM, and a cOmplete™ protease inhibitor tablet/L). A stepwise
334 gradient of increasing concentrations of NaCl (from 0 to 1 M NaCl) was applied and the fractions eluted
335 at 0.45 M and 0.5 M NaCl were pooled, concentrated and the ionic strength of the solution was lowered
336 by dilution with buffer A and ultrafiltration (50 kDa cutoff, Amicon, Millipore). The concentrate was
337 applied to a Resource Q column (1.6 x 3.0 cm, Amersham Pharmacia Biotech) equilibrated with buffer A.

338 A stepwise gradient of increasing concentrations of NaCl (from 0 to 1 M NaCl) was performed and the
339 fractions eluted at 0.3 M and 0.35 M NaCl were pooled, concentrated and the ionic strength lowered by
340 dilution and concentration steps as above. All the chromatographic steps were performed at 4 °C, at air,
341 and monitored by UV-visible spectroscopy. The purity of DsrMKJOP was analyzed by a 10% Tricine-SDS-
342 PAGE gel and a Blue Native (BN)-PAGE gel, followed by Coomassie Blue staining and heme-staining (33),
343 and the protein concentration was determined using the previously determined absorption coefficient (ε)
344 of 132.4 $mM^{-1}.cm^{-1}$ at 555 nm in the reduced state (34).
345
346 **UV-visible Spectroscopy**
347 UV–visible spectra were acquired in a Shimadzu UV-1800 spectrophotometer inside a Coy anaerobic
348 chamber (98 % N_2, 2 % H_2). Spectra were obtained at 60 °C, using as-purified DsrMKJOP, prepared in 20
349 mM Tris-HCl pH 7.5, then incubated with menadiol and an excess of sodium dithionite to allow full
350 reduction. Menadiol was prepared by reduction of menadione with sodium dithionite (35), stored in dry
351 state at -20 °C under anaerobic conditions, and solubilized in ethanol prior to use. A control spectrum of
352 the as-purified DsrMKJOP complex was obtained by addition of the same volume of ethanol as for
353 menadiol incubation.
354
355 **Electron Paramagnetic Resonance Spectroscopy**
356 X-band electron paramagnetic resonance (EPR) spectra were obtained on a Bruker EMX spectrometer
357 (Billerica, MA) equipped with an Oxford Instruments ESR-900 continuous flow helium cryostat (Abingdon,
358 UK). A menadiol-treated sample of the DsrMKJOP complex, in 20 mM Tris-HCl pH 7.5 at a concentration
359 of 25 µM, was prepared inside a Coy anaerobic chamber (98 % N_2, 2 % H_2) by incubation for 2h at 60 °C
360 with a solution of menadiol in ethanol in a 1:500 ratio. As control an as-purified DsrMKJOP sample was
361 also incubated for 2 h with the same volume of ethanol as was used in the menadiol experiment. Samples
362 were transferred to EPR tubes within the anaerobic chamber, capped, and immediately frozen in liquid
363 nitrogen upon removal from the chamber. All spectra were recorded using a microwave frequency of 9.38
364 GHz, a field modulation frequency of 100 kHz, a microwave power of 20.1 mW, a modulation amplitude
365 of 1.0 mT, and a temperature of 23 K.
366
367 **Purification of *A. fulgidus* DsrAB**
368 The purification protocol of the soluble extract from *A. fulgidus* cells followed two consecutive ion
369 exchange chromatography steps at 4 °C under air, as described in detail in Santos *et al.* (7). The purity of
370 DsrAB was analyzed in a 10% Tricine-SDS-PAGE gel, and the protein concentration was determined by UV-
371 visible spectroscopy using an ε of 60 $mM^{-1}.cm^{-1}$ at 593 nm determined previously (36). The purified DsrAB
372 was stored under anaerobic conditions to prevent prolonged contact with O_2, which leads to gradual
373 activity loss.
374
375 **Purification of Recombinant *A. fulgidus* DsrC**
376 *A. fulgidus* DsrC with the two structural Cys (Cys^{77} and Cys^{85}) modified to Ala was expressed in *Escherichia*
377 *coli* and purified by an affinity exchange chromatography step on a HiTrap™ immobilized metal-ion affinity
378 chromatography (IMAC) high performance column (GE Healthcare), as described in detail in Ferreira *et al.*
379 (9). The purity of DsrC was analyzed on a 10% Tricine-SDS-PAGE gel, and the protein concentration was

380 determined by bicinchoninic acid (BCA) assay (Merck Millipore) and by UV-visible spectroscopy using an ε
381 of 24 $mM^{-1}\cdot cm^{-1}$ at 280 nm. Before its use in activity assays, DsrC was treated with 5 mM dithiothreitol
382 (DTT, Sigma-Aldrich) during 30 min at 37 °C, to ensure its Cys were in the reduced state, and excess
383 reductant was removed with a HiTrap™ Desalting column (GE Healthcare) (7). Reduced DsrC was
384 concentrated, if necessary, by ultrafiltration (10 kDa cutoff, Amicon Millipore) and kept under anaerobic
385 conditions until use. The redox state of the DsrC (5 µg) was analyzed by a gel-shift assay using MalPEG
386 (methoxy-polyethylene glycol maleimide, Fluka), as described in Venceslau *et al.* (37).
387
388 **Production and Analysis of DsrC-trisulfide**
389 The enzymatic production of DsrC-trisulfide was performed inside a Coy anaerobic chamber (98% N_2, 2%
390 H_2) at 60 °C using Zn-reduced methyl viologen (Sigma-Aldrich) as the electron donor (7). The activity assays
391 were run in 50 mM KPi pH 7.0, 1 mM Zn-reduced methyl viologen (MV^+), 200 nM of DsrAB, 0.5 mM sodium
392 sulfite (Sigma-Aldrich), with a range from 10 µM to 100 µM of reduced DsrC. After a 5 min incubation of
393 DsrAB in the reaction buffer, followed by a 1 min incubation with DsrC, the reaction was started by
394 addition of sodium sulfite. The oxidation of MV^+ was monitored at 732 nm (ε = 3.15 $mM^{-1}\cdot cm^{-1}$) in a
395 spectrophotometer. A prolonged incubation time (from 15 to 60 min depending on the DsrC-trisulfide
396 concentration) was used to try to drive the enzymatic reaction to completion and have DsrC as much as
397 possible in the trisulfide form. The enzymatic solution was diluted and concentrated by ultrafiltration (10
398 kDa cutoff, Amicon Millipore) to remove the methyl viologen. The redox state of DsrC was monitored with
399 the MalPEG gel-shift assay as previously described (37).
400
401 **Determination of DsrC Thiol Content by DTNB**
402 DsrC in different redox states was subject to a DTNB (5,5-dithio-bis-(2-nitrobenzoic acid) – Ellman's
403 reagent) assay to quantify the sulfhydryl groups present. DsrC (0.8 – 3 nmol) was incubated in 100 mM
404 KPi pH 8.0, 1 mM EDTA, and 0.2 mM DTNB (Sigma-Aldrich) for 15 min at room temperature. The
405 production of 2-nitro-5-thiobenzoate anion (TNB^{2-}) was quantified by measuring the absorbance at 412
406 nm using the ε of 14150 $M^{-1}\cdot cm^{-1}$ (38).
407
408 **Surface Plasmon Resonance Analysis**
409 The surface plasmon resonance (SPR) experiments were performed at 25 °C on a BIAcore 2000 instrument
410 (GE Healthcare). DsrC-trisulfide was immobilized on a NTA sensor chip (GE Healthcare) by the His-tag tail
411 present at the N terminus. All the assays were performed with 10 mM HEPES pH 7.4, 150 mM NaCl, 50
412 µM EDTA, and 0.005% (v/v) Tween 20 running buffer. DsrC-trisulfide (45 nM) was bound to a previously
413 activated flow cell at a flow rate of 5 µL/min in the presence of 500 µM $NiCl_2$ in running buffer in order to
414 have an immobilization of around 350 resonance units (RU). Another activated flow cell was similarly
415 treated with running buffer in the absence of DsrC-trisulfide (control cell). Interaction experiments with
416 DsrMKJOP complex were performed with a 3 min injection of increasing concentrations of DsrMKJOP
417 complex (range from 8.9 nM to 568 nM) at a flow rate of 30 µL/min. At the end of sample injection, the
418 NTA sensor chip was regenerated with 350 mM EDTA in running buffer for 1 min at a flow rate of 10
419 µL/min before a new cycle of surface activation and immobilization. Sensorgrams were obtained by
420 subtracting the unspecific binding to the control flow cell in order to remove buffer artifacts and

421 normalizing to the baseline injection timepoint. The equilibrium dissociation constant (K_D) was
422 determined from duplicate experiments and according to $RU_{steady\text{-}state} = (RU_{max} \times [analyte])/K_D + [analyte])$.
423
424 **DsrMKJOP Activity Assays**
425 Menadiol:DsrC-trisulfide oxidoreductase activity assays by DsrMKJOP were performed inside a Coy
426 anaerobic chamber (98% N_2, 2% H_2) at 60 °C using menadiol as electron donor. The activity assays were
427 run in 50 mM KPi pH 7.0, 0.5 mM menadiol, and 100 nM DsrMKJOP in the presence of DsrC-trisulfide (10
428 µM). The reaction was started by addition of DsrC-trisulfide after a 5 min incubation of DsrMKJOP in the
429 reaction buffer. The oxidation of menadiol was monitored at 270 nm (using $\varepsilon_{DMN} = 16\ mM^{-1}\cdot cm^{-1}$ (39)) in
430 a spectrophotometer. For peptide mass fingerprinting of DsrC, the enzymatic reactions were
431 concentrated and dialyzed by ultrafiltration (10 kDa cutoff, Amicon Millipore). To monitor the redox state
432 of DsrC cysteines, the MalPEG gel-shift assay was used (37).
433
434 **Peptide Mass Fingerprinting**
435 The redox state of DsrC cysteines was analyzed by peptide mass fingerprinting using a matrix-assisted
436 laser desorption/ionization-time-of-flight (MALDI-TOF/TOF) mass spectrometer, as described in Santos *et*
437 *al.* (7). Alkylation was performed inside an anaerobic chamber by incubation of DsrC with 50 mM
438 iodoacetamide (IA, Sigma-Aldrich) in 50 mM ammonium bicarbonate pH 7.8 during 30 min at 55 °C and
439 run on a 10% Tricine-SDS-PAGE gel (15 µg) under non-reducing conditions. The protein bands were
440 excised, destained and digested with Asp-N (Roche, 20 ng/µL) overnight at 37 °C. This endoproteinase
441 generates a peptide comprising both conserved C-terminal cysteine residues, ^{101}DA**C**RIAGLPKPTG**C**V^{115},
442 with predicted mass of 1500.8 Daltons (Da). The digested peptides were desalted and concentrated using
443 POROS C18 (Empore, 3M) and eluted directly onto the MALDI plate using 1 µL of 5 mg/mL alpha-cyano-4-
444 hydroxycinnamic acid (CHCA, Sigma-Aldrich) in 50% (v/v) acetonitrile and 5% (v/v) formic acid.
445 The data were acquired in positive reflector MS mode using a 5800 MALDI-TOF/TOF (AB Sciex) mass
446 spectrometer and TOF/TOF Series Explorer Software v.4.1.0 (Applied Biosystems). External calibration was
447 performed using CalMix5 (Protea). Mass Spectrometry (MS) data were analyzed using Data Explorer
448 Software v.4.11 (AB Sciex) and obtained at the Mass Spectrometry Unit (UniMS), ITQB/iBET, Oeiras,
449 Portugal.
450
451 **Determination of Hydrogen Sulfide by HPLC**
452 Hydrogen sulfide was quantified using monobromobimane (mBBr) derivatization (40). mBBr (Thermo
453 Fisher Scientific) was diluted in HPLC ultrapure acetonitrile to a final concentration of 50 mM. For
454 derivatization, 10 µL of sample from the enzymatic reaction were reacted with 3 µL of mBBr in 50 mM
455 EPPS (4-(2-hydroxyethyl)piperazine-1-propanesulfonic acid) pH 8.0 and 5 mM DTPA
456 (diethylenetriaminepentaacetic acid) in a final volume of 86 µL, inside an anaerobic chamber. The
457 reactions were incubated in the dark at room temperature for 10 min, after which 4 µL of 5 M
458 methanesulfonic acid was added to stop the reaction. Derivatized hydrogen sulfide (sulfide dibimane) was
459 measured by high performance liquid chromatography (HPLC, Waters Alliance 2695) with a fluorescence
460 detector (Waters 2475) with an excitation/emission wavelength of 380 and 480 nm, respectively, using a
461 reverse phase Ultrasphere® ODS column (4.6 x 250 mm, 5 µm, Hichrom) run at a flow rate of 1.2 $mL\cdot min^{-1}$
462 and 35 °C, as described in detail in Santos *et al.* (7). The retention time was 15.5 min for sulfide dibimane.

463 A calibration curve was performed with freshly prepared solutions of sodium sulfide nonahydrate (Sigma-
464 Aldrich) in 50 mM KPi pH 7.0, reacted with excess mBBr.
465
466 **ACKNOWLEDGEMENTS**
467 We thank João Carita and Cristina Leitão from ITQB NOVA for the growth of *A. fulgidus* and HPLC analysis,
468 respectively. This work was funded by the Fundação para a Ciência e Tecnologia (Portugal) through
469 Fellowships PD/BD/135488/2018 and COVID/BD/152504/2022 (A.C.C.B.), Grants PTDC/BIA-
470 MIC/6512/2014 and PTDC/BIA-BQM/29118/2017, Research Unit Molecular, Structural and Cellular
471 Microbiology (MOSTMICRO-ITQB) (UIDB/04612/2020 and UIDP/04612/2020), and Associate Laboratory
472 Life Sciences for a Healthy and Sustainable Future (LS4FUTURE) (LA/P/0087/2020).
473
474
475

476 **REFERENCES**

477 1. G. Muyzer, A. J. M. Stams, The ecology and biotechnology of sulphate-reducing bacteria. *Nat. Rev.*
478 *Microbiol.* **6**, 441–454 (2008).
479 2. R. Rabus, *et al.*, A Post-Genomic View of the Ecophysiology, Catabolism and Biotechnological
480 Relevance of Sulphate-Reducing Prokaryotes. *Adv. Microb. Physiol.* **66**, 55–321 (2015).
481 3. B. B. Jørgensen, A. J. Findlay, A. Pellerin, The biogeochemical sulfur cycle of marine sediments.
482 *Front. Microbiol.* **10**, 1–27 (2019).
483 4. S. E. McGlynn, G. L. Chadwick, C. P. Kempes, V. J. Orphan, Single cell activity reveals direct electron
484 transfer in methanotrophic consortia. *Nature* **526**, 531–535 (2015).
485 5. G. Wegener, V. Krukenberg, D. Riedel, H. E. Tegetmeyer, A. Boetius, Intercellular wiring enables
486 electron transfer between methanotrophic archaea and bacteria. *Nature* **526**, 587–590 (2015).
487 6. D. E. Canfield, M. T. Rosing, C. Bjerrum, Early anaerobic metabolisms. *Philos. Trans. R. Soc. B Biol.*
488 *Sci.* **361**, 1819–1836 (2006).
489 7. A. A. Santos, *et al.*, A protein trisulfide couples dissimilatory sulfate reduction to energy
490 conservation. *Science.* **350**, 1541–1545 (2015).
491 8. T. F. Oliveira, *et al.*, The crystal structure of *Desulfovibrio vulgaris* dissimilatory sulfite reductase
492 bound to DsrC provides novel insights into the mechanism of sulfate respiration. *J. Biol. Chem.* **283**,
493 34141–34149 (2008).
494 9. D. Ferreira, *et al.*, The DsrD functional marker protein is an allosteric activator of the DsrAB
495 dissimilatory sulfite reductase. *Proc. Natl. Acad. Sci. U. S. A.* **119** (2022).
496 10. S. S. Venceslau, Y. Stockdreher, C. Dahl, I. A. C. Pereira, The "bacterial heterodisulfide" DsrC is a
497 key protein in dissimilatory sulfur metabolism. *Biochim. Biophys. Acta - Bioenerg.* **1837**, 1148–1164
498 (2014).
499 11. R. H. Pires, *et al.*, Characterization of the *Desulfovibrio desulfuricans* ATCC 27774 DsrMKJOP
500 complex - A membrane-bound redox complex involved in the sulfate respiratory pathway.
501 *Biochemistry* **45**, 249–262 (2006).
502 12. A. S. Pott, C. Dahl, Sirohaem sulfite reductase and other proteins encoded by genes at the dsr locus
503 of *Chromatium vinosum* are involved in the oxidation of intracellular sulfur. *Microbiology* **144**,
504 1881–1894 (1998).
505 13. C. Dahl, A biochemical view on the biological sulfur cycle. *Environ. Technol. to Treat Sulphur Pollut.*
506 *Princ. Eng.*, 55–96 (2020).
507 14. J. Simon, P. M. H. Kroneck, Microbial Sulfite Respiration. *Adv. Microb. Physiol.* **62**, 45–117 (2013).
508 15. K. Wasmund, M. Mußmann, A. Loy, The life sulfuric: microbial ecology of sulfur cycling in marine
509 sediments. *Environ. Microbiol. Rep.* **9**, 323–344 (2017).
510 16. G. J. Mander, E. C. Duin, D. Linder, K. O. Stetter, R. Hedderich, Purification and characterization of
511 a membrane-bound enzyme complex from the sulfate-reducing archaeon *Archaeoglobus fulgidus*
512 related to heterodisulfide reductase from methanogenic archaea. *Eur. J. Biochem.* **269**, 1895–1904
513 (2002).
514 17. F. Grein, I. A. C. Pereira, C. Dahl, Biochemical characterization of individual components of the
515 *Allochromatium vinosum* DsrMKJOP transmembrane complex aids understanding of complex
516 function in vivo. *J. Bacteriol.* **192**, 6369–6377 (2010).
517 18. J. Sander, S. Engels-Schwarzlose, C. Dahl, Importance of the DsrMKJOP complex for sulfur oxidation

518 in *Allochromatium vinosum* and phylogenetic analysis of related complexes in other prokaryotes.
519 *Arch. Microbiol.* **186**, 357–366 (2006).
520 19. I. A. C. Pereira, *et al.*, A comparative genomic analysis of energy metabolism in sulfate reducing
521 bacteria and archaea. *Front. Microbiol.* **2**, 25–36 (2011).
522 20. S. Heiden, R. Hedderich, E. Setzke, R. K. Thauer, Purification of a two-subunit cytochrome-*b*-
523 containing heterodisulfide reductase from methanol-grown *Methanosarcina barkeri*. *Eur. J.*
524 *Biochem.* **221**, 855–861 (1994).
525 21. A. Künkel, M. Vaupel, S. Heim, R. K. Thauer, R. Hedderich, Heterodisulfide reductase from
526 methanol-grown cells of *Methanosarcina barkeri* is not a flavoenzyme. *Eur. J. Biochem.* **244**, 226–
527 234 (1997).
528 22. R. Hedderich, N. Hamann, M. Bennati, Heterodisulfide reductase from methanogenic archaea: A
529 new catalytic role for iron-sulfur cluster. *Biol. Chem.* **386**, 961–970 (2005).
530 23. N. Hamann, *et al.*, A cysteine-rich CCG domain contains a novel [4Fe-4S] cluster binding motif as
531 deduced from studies with subunit B of heterodisulfide reductase from *Methanothermobacter*
532 *marburgensis*. *Biochemistry* **46**, 12875–12885 (2007).
533 24. A. G. Duarte, *et al.*, Redox loops in anaerobic respiration - The role of the widespread NrfD protein
534 family and associated dimeric redox module. *Biochim. Biophys. Acta - Bioenerg.* **1862**, 148416
535 (2021).
536 25. F. Grein, *et al.*, DsrJ, an essential part of the DsrMKJOP transmembrane complex in the purple
537 sulfur bacterium *Allochromatium vinosum*, is an unusual triheme cytochrome *c*. *Biochemistry* **49**,
538 8290–8299 (2010).
539 26. M. R. Cheesman, P. J. Little, B. C. Berks, Novel heme ligation in a *c*-type cytochrome involved in
540 thiosulfate oxidation: EPR and MCD of SoxAX from *Rhodovulum sulfidophilum*. *Biochemistry* **40**,
541 10562–10569 (2001).
542 27. K. Denkmann, *et al.*, Thiosulfate dehydrogenase: A widespread unusual acidophilic *c*-type
543 cytochrome. *Environ. Microbiol.* **14**, 2673–2688 (2012).
544 28. J. Alric, *et al.*, Structural and functional characterization of the unusual triheme cytochrome bound
545 to the reaction center of *Rhodovulum sulfidophilum*. *J. Biol. Chem.* **279**, 26090–26097 (2004).
546 29. F. Grein, A. R. Ramos, S. S. Venceslau, I. A. C. Pereira, Unifying concepts in anaerobic respiration:
547 Insights from dissimilatory sulfur metabolism. *Biochim. Biophys. Acta - Bioenerg.* **1827**, 145–160
548 (2013).
549 30. T. Wagner, J. Koch, U. Ermler, S. Shima, Methanogenic heterodisulfide reductase (HdrABC-
550 MvhAGD) uses two noncubane [4Fe-4S] clusters for reduction. *Science.* **357**, 699–703 (2017).
551 31. V. Pelmenschikov, *et al.*, Substrate-Dependent Conformational Switch of the Noncubane [4Fe-4S]
552 Cluster in Heterodisulfide Reductase HdrB. *J. Am. Chem. Soc.* **145**, 7–11 (2023).
553 32. K. O. Stetter, G. Lauerer, M. Thomm, A. Neuner, Isolation of Extremely Thermophilic Sulfate
554 Reducers: Evidence for a Novel Branch of Archaebacteria. *Science.* **236**, 822–824 (1987).
555 33. R. T. Francis, R. R. Becker, Specific indication of hemoproteins in polyacrylamide gels using a
556 double-staining process. *Anal. Biochem.* **136**, 509–514 (1984).
557 34. Venceslau S. S., "Electron transfer chains in sulfate reducing bacteria." Instituto de Tecnologia
558 Química e Biológica António Xavier, Universidade Nova de Lisboa. Ph.D. Thesis Dissertation (2011).
559 35. L. F. Fieser, Convenient Procedures for the Preparation of Antihemorrhagic Compounds. *J. Biol.*

560 *Chem.* **133**, 391–396 (1940).
561 36. C. Dahl, N. M. Kredich, R. Deutzmann, H. G. Truper, Dissimilatory sulphite reductase from
562 *Archaeoglobus fulgidus*: Physico-chemical properties of the enzyme and cloning, sequencing and
563 analysis of the reductase genes. *J. Gen. Microbiol.* **139**, 1817–1828 (1993).
564 37. S. S. Venceslau, *et al.*, Redox states of *Desulfovibrio vulgaris* DsrC, a key protein in dissimilatory
565 sulfite reduction. *Biochem. Biophys. Res. Commun.* **441**, 732–736 (2013).
566 38. P. W. Riddles, R. L. Blakeley, B. Zerner, Reassessment of Ellman's Reagent. *Methods Enzymol.* **91**,
567 49–60 (1983).
568 39. J. H. Weiner, *et al.*, A mutant of *Escherichia coli* fumarate reductase decoupled from electron
569 transport. *Proc. Natl. Acad. Sci.* **83**, 2056–2060 (1986).
570 40. R. C. Fahey, G. L. Newton, Determination of Low-Molecular-Weight Thiols Using
571 Monobromobimane Fluorescent Labeling and High-Performance Liquid Chromatography.
572 *Methods Enzymol.* **143**, 85–96 (1987).
573 41. S. Madadi-Kahkesh, *et al.*, A paramagnetic species with unique EPR characteristics in the active site
574 of heterodisulfide reductase from methanogenic archaea. *Eur. J. Biochem.* **268**, 2566–2577 (2001).
575 42. E. C. Duin, C. Bauer, B. Jaun, R. Hedderich, Coenzyme M binds to a [4Fe-4S] cluster in the active
576 site of heterodisulfide reductase as deduced from EPR studies with the [^{33}S]coenzyme M-treated
577 enzyme. *FEBS Lett.* **538**, 81–84 (2003).
578 43. E. C. Duin, S. Madadi-Kahkesh, R. Hedderich, M. D. Clay, M. K. Johnson, Heterodisulfide reductase
579 from *Methanothermobacter marburgensis* contains an active-site [4Fe-4S] cluster that is directly
580 involved in mediating heterodisulfide reduction. *FEBS Lett.* **512**, 263–268 (2002).
581 44. D. P. Bhave, J. A. Hong, R. L. Keller, C. Krebs, K. S. Carroll, Iron-sulfur cluster engineering provides
582 insight into the evolution of substrate specificity among sulfonucleotide reductases. *ACS Chem.*
583 *Biol.* **7**, 306–315 (2012).
584 45. M. Rossi, *et al.*, The hmc operon of *Desulfovibrio vulgaris* subsp. *vulgaris* Hildenborough encodes
585 a potential transmembrane redox protein complex. *J. Bacteriol.* **175**, 4699–4711 (1993).
586 46. P. M. Pereira, M. Teixeira, A. V. Xavier, R. O. Louro, I. A. C. Pereira, The Tmc complex from
587 *Desulfovibrio vulgaris* Hildenborough is involved in transmembrane electron transfer from
588 periplasmic hydrogen oxidation. *Biochemistry* **45**, 10359–10367 (2006).
589 47. M. Tietze, *et al.*, Redox potentials of methanophenazine and CoB-S-S-CoM, factors involved in
590 electron transport in methanogenic archaea. *ChemBioChem* **4**, 333–335 (2003).
591 48. S. E. Chobot, H. H. Hernandez, C. L. Drennan, S. J. Elliott, Direct Electrochemical Characterization
592 of Archaeal Thioredoxins. *Angew. Chemie Int. Ed.* **46**, 4145–4147 (2007).
593 49. A. Zöphel, M. C. Kennedy, H. Beinert, P. M. H. Kroneck, Investigations on microbial sulfur
594 respiration. *Arch. Microbiol.* **150**, 72–77 (1988).
595 50. L. Flohé, The fairytale of the GSSG/GSH redox potential. *Biochim. Biophys. Acta - Gen. Subj.* **1830**,
596 3139–3142 (2013).
597 51. C. Berndt, C. H. Lillig, L. Flohé, Redox regulation by glutathione needs enzymes. *Front. Pharmacol.*
598 **5** (2014).
599 52. V. A. Bamford, *et al.*, Structural basis for the oxidation of thiosulfate by a sulfur cycle enzyme.
600 *EMBO J.* **21**, 5599–5610 (2002).
601 53. A. G. Duarte, *et al.*, An electrogenic redox loop in sulfate reduction reveals a likely widespread

602 mechanism of energy conservation. *Nat. Commun.* **9**, 5448 (2018).
603 54. J. S. Sousa, *et al.*, Structural basis for energy transduction by respiratory alternative complex III.
604 *Nat. Commun.* **9**, 1728 (2018).
605 55. C. Sun, *et al.*, Structure of the alternative complex III in a supercomplex with cytochrome oxidase.
606 *Nature* **557**, 123–126 (2018).
607 56. A. Kublik, *et al.*, Identification of a multi-protein reductive dehalogenase complex in D
608 ehalococcoides mccartyi strain CBDB1 suggests a protein-dependent respiratory electron
609 transport chain obviating quinone involvement. *Environ. Microbiol.* **18**, 3044–3056 (2016).
610

611 **Figure Legends**

612

613 **Figure 1 – UV-visible and EPR spectroscopy of the *A. fulgidus* DsrMKJOP complex.** (A) UV-visible spectra
614 of as-purified DsrMKJOP (blue), menadiol-reduced (red), and dithionite-reduced (green). (B) EPR spectra
615 of the $[4Fe\text{-}4S]^{3+/2+}$ cluster of the as-purified DsrMKJOP (blue), and upon menadiol reduction (red). *g*-
616 values are marked in the spectrum of as-purified DsrMKJOP. All menadiol reduction spectra were obtained
617 in a 1:500 protein to menadiol ratio.

618

619 **Figure 2 – Interaction assays between DsrC-trisulfide and DsrMKJOP complex.** Sensorgrams of DsrC-
620 trisulfide interaction with increasing concentrations of DsrMKJOP (8.9 nM to 568 nM) using SPR.
621 Sensorgrams were measured in duplicate.

622

623 **Figure 3 – Kinetic assays of the effect of DsrC-trisulfide on DsrMKJOP activity.** (A) Menadiol:DsrC-
624 trisulfide oxidoreductase activity catalyzed by *A. fulgidus* DsrMKJOP (blue), and in the absence of DsrC-
625 trisulfide (purple), absence of DsrMKJOP (red), and absence of menadiol (green). (B) Menadiol:DsrC-
626 trisulfide oxidoreductase activity catalyzed by *A. fulgidus* DsrMKJOP upon successive additions of DsrC-
627 trisulfide (arrow indicates addition of 5 µM DsrC-trisulfide). (C and D) Gel-shift analysis of MalPEG-labeled
628 DsrC from (A) and after reaction with DsrMKJOP and 0.5 mM menadiol over time (at 0, 1, 2, 3, 5, 10, 15,
629 20 and 30 min), respectively. MalPEG causes a shift of approximately 10 kDa per each labeled cysteine.
630 (E) Gel-shift analysis of MalPEG-labeled DsrC with increasing concentrations of menadiol (0, 0.8, 4, 20, 100
631 and 500 µM), reacted for 30 mins. (M, molecular marker; T_0, time zero; T_f, time at the end of reaction).

632

633 **Figure 4 – Peptide mass fingerprinting spectra of DsrC C-terminal peptides after alkylation with IA.** (A)
634 DTT-reduced DsrC (before the reaction with *A. fulgidus* DsrAB and sulfite). (B) DsrC-trisulfide (produced in
635 the *in vitro* enzymatic reaction with *A. fulgidus* DsrAB and sulfite). (C) DsrC recovered after the *in vitro*
636 enzymatic reaction with *A. fulgidus* DsrMKJOP complex and menadiol. The C-terminal peptide of DsrC-
637 trisulfide (1530.7 Da) is marked with an arrow in (C) showing its disappearance from (B) to (C). (IA,
638 iodoacetamide; DTT, dithiothreitol).

639

640 **Figure 5 – Reduction of DsrC-trisulfide by DsrMKJOP and sulfide production.** (A) Schematic
641 representation of the reaction catalyzed by DsrMKJOP. (B) Menadiol:DsrC-trisulfide oxidoreductase
642 activity catalyzed by *A. fulgidus* DsrMKJOP with increasing concentrations of DsrC-trisulfide (0 µM to 10
643 µM). (C) Hydrogen sulfide produced in the reactions shown in (B). H_2S was measured before the addition
644 of DsrC-trisulfide (T_0) and 30 min after the start of the enzymatic reaction (T_f). The control in the absence
645 of DsrC-trisulfide was subtracted from all points. Results from a representative experiment are shown.

646

647

648 **Figure 1**

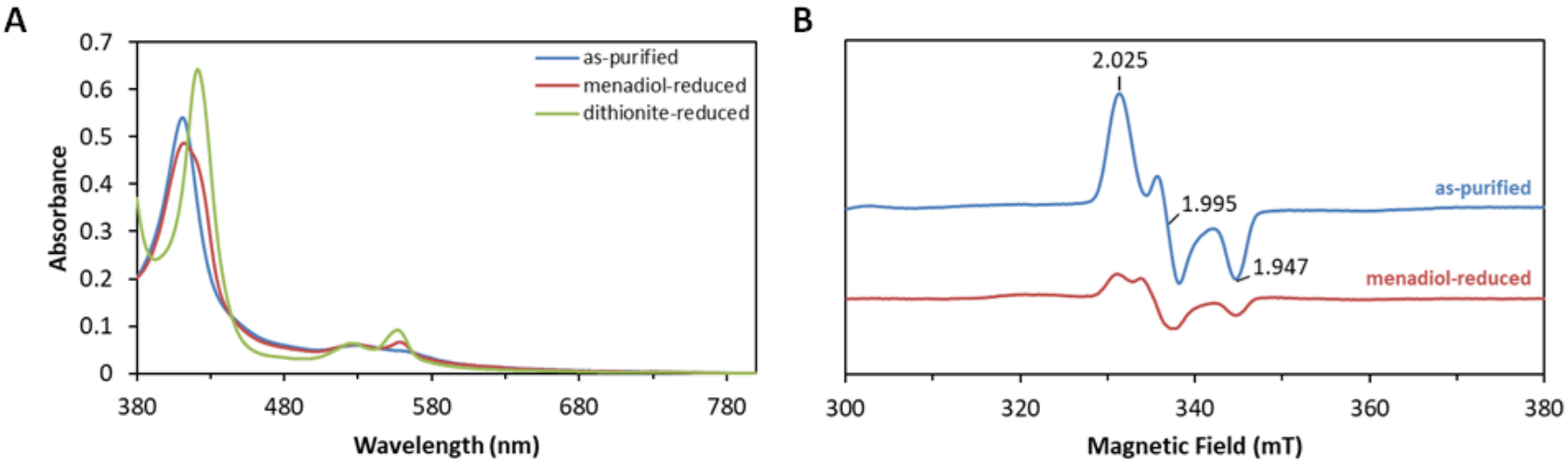

649

650 **Figure 2**

651

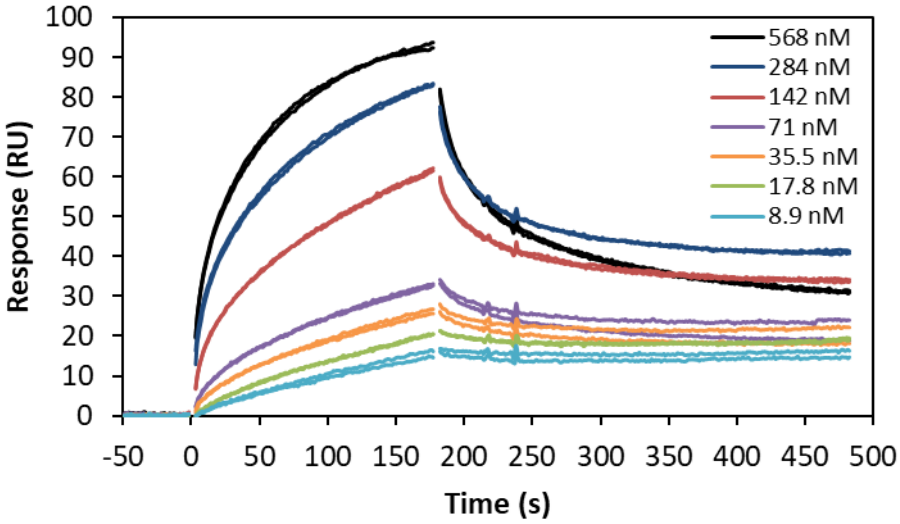

652

653 **Figure 3**

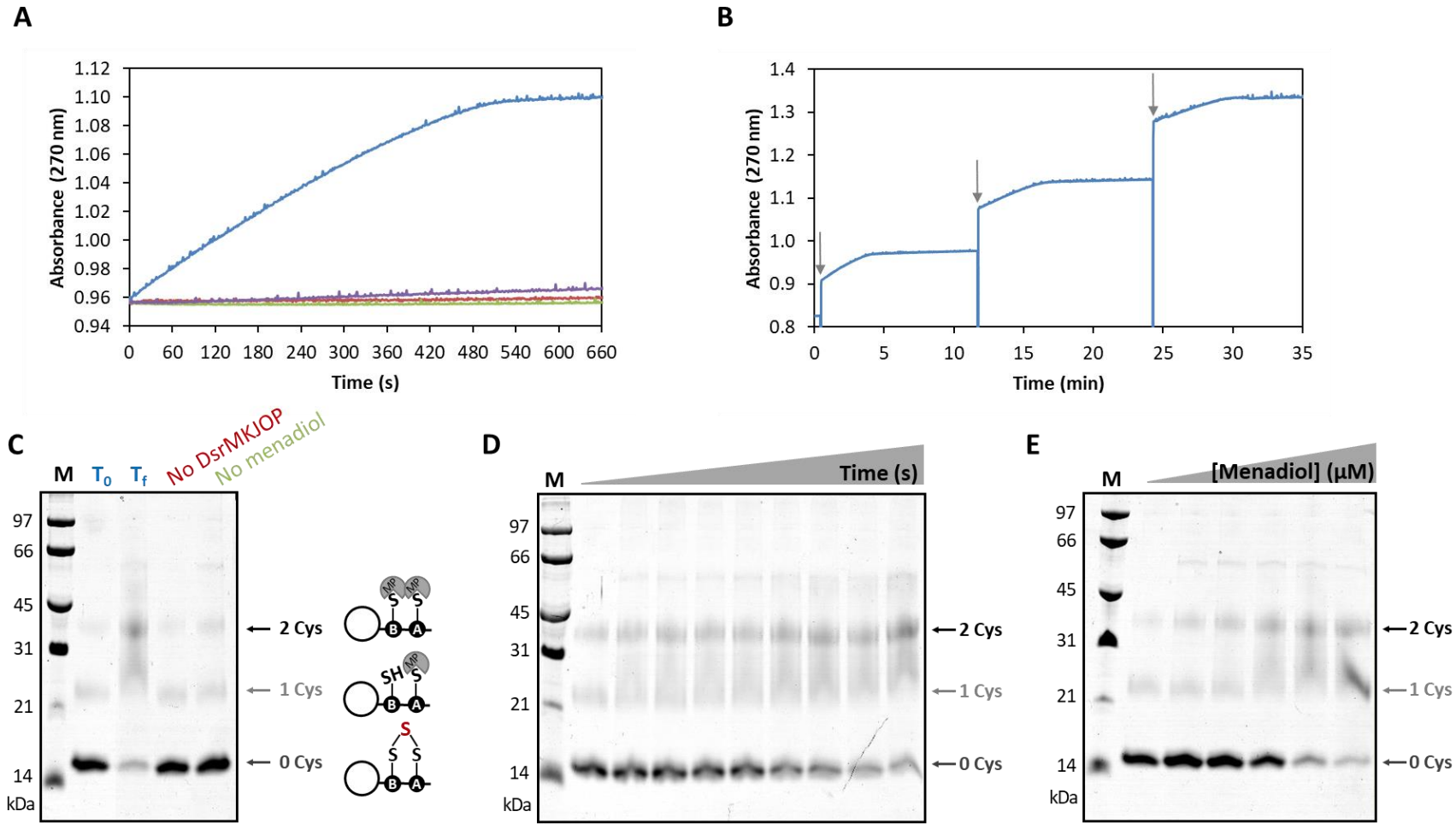

654

655

656

657

658 **Figure 4**

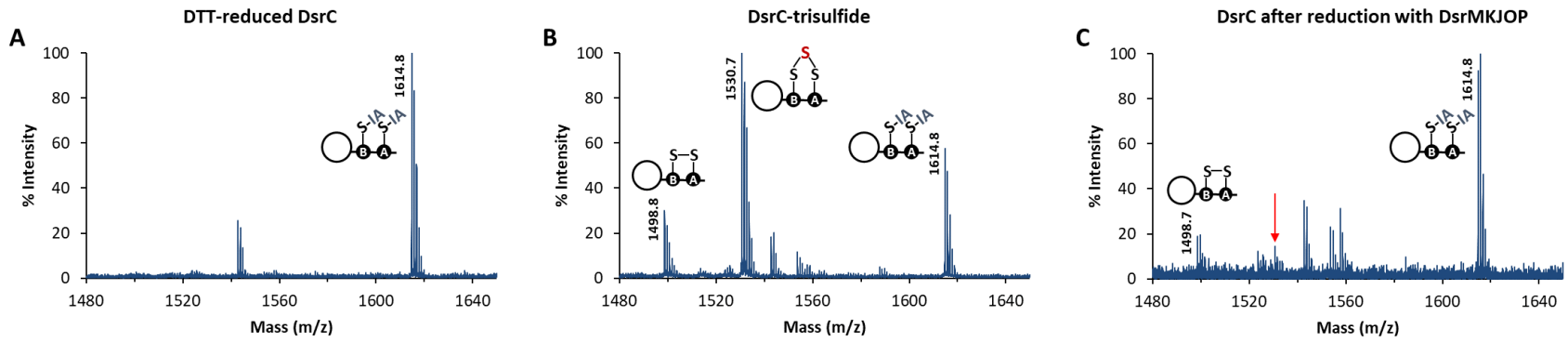

659

660

661

662

663

664

665

666

667

668

669

670

671

672 **Figure 5**

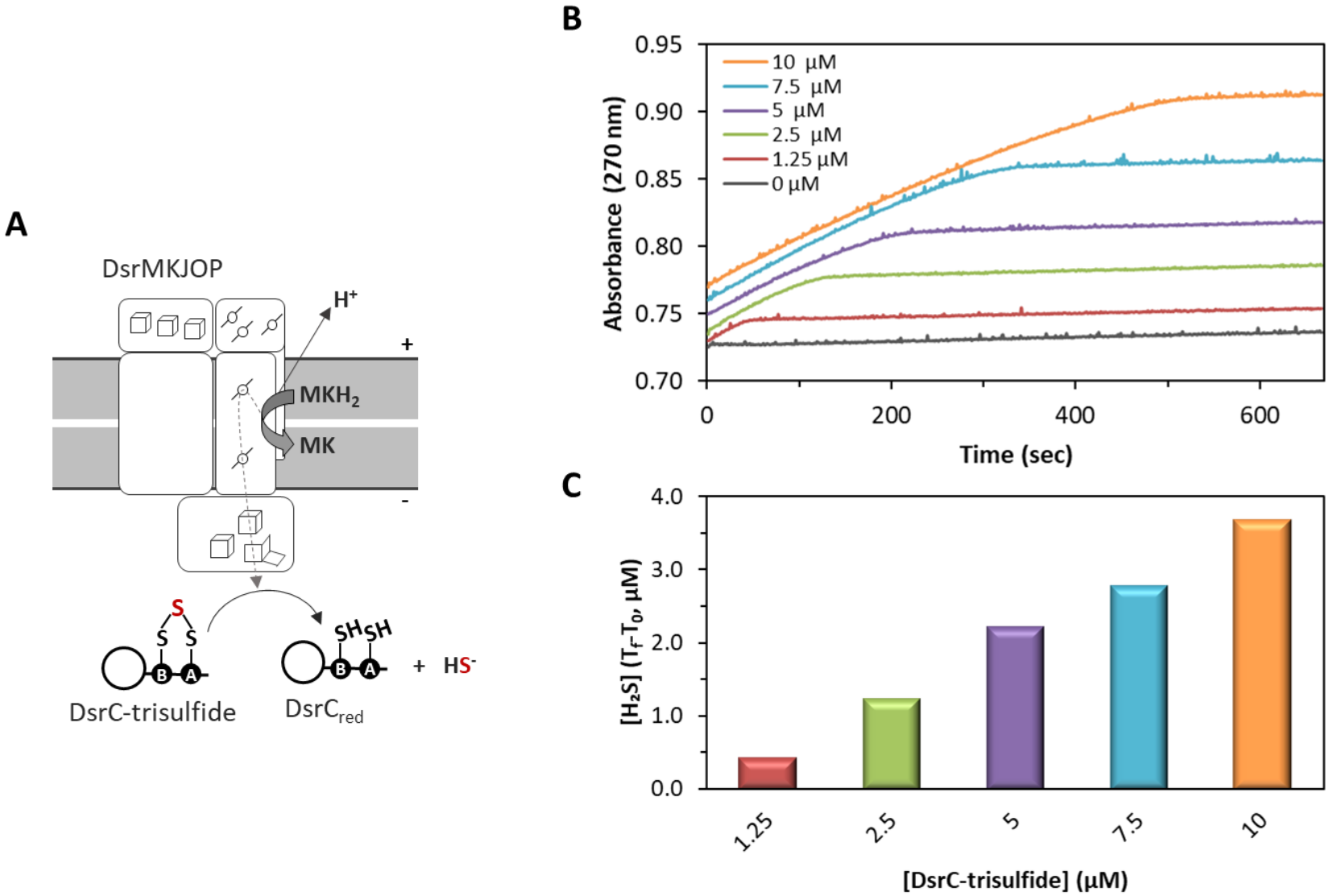

673